ARMY RESEARCH LABORATORY

High-Sensitivity Wideband Analog Fiber-Optic Link Based on Integrated Optical Modulators

by Bruce T. Benwell,
U.S. Army Research Laboratory

Daniel Edmands and Eduardo Saravia
Interscience, Inc.

ARL-TR-1188 January 1997

The findings in this report are not to be construed as an official Department of the Army position unless so designated by other authorized documents.

Citation of manufacturer's or trade names does not constitute an official endorsement or approval of the use thereof.

Destroy this report when it is no longer needed. Do not return it to the originator.

Army Research Laboratory
Adelphi, MD 20783-1197

ARL-TR-1188 **January 1997**

High-Sensitivity Wideband Analog Fiber-Optic Link Based on Integrated Optical Modulators

Bruce T. Benwell
Sensors and Electron Devices Directorate, ARL

Daniel Edmands and Eduardo Saravia
Interscience, Inc.

Abstract

This report summarizes the design and testing of a 10-GHz analog fiber-optic link. The device is based on a state-of-the-art, commercially available $LiNbO_3$ electro-optic integrated Mach-Zehnder modulator. The performance of the integrated link, as well as each individual component, is characterized and documented.

Contents

Figures

Table

1. Introduction

Fiber-optic links are being used increasingly to transmit analog and digital signals at radio and microwave frequencies. Compared to waveguides and coax cables, fiber-optic links rate higher for being wider bandwidth, lower loss, and lighter weight, and they have a natural immunity to electromagnetic interference (EMI) and eavesdropping.

The U.S. Army Research Laboratory (ARL) is developing, through the Small Business Innovative Research (SBIR) Program, a wideband fiber-optic transmission systems that will avoid contamination of measured signals in an intense ambient electromagnetic environment during radio frequency (rf) experimentation. For this particular application, the fiber-optic link specifications include a bandwidth from 10 kHz to 5 GHz, minimum sensitivity of 100 μV (at tangential noise), and a dynamic range of 40 dB, using fiber lengths at least 200 m long. These specifications require a major advance over the present state-of-the-art for miniature fieldable fiber-optic links.

The principal objective of the work described in this report was to evaluate the feasibility of and develop a design for a wide-bandwidth analog fiber-optic link, based on the phase modulation of an external laser. The primary advantage of using this new technique is that modulation frequencies as high as 50 GHz appear to be attainable with presently available commercial electro-optic integrated modulators (EOIM). In particular, recent advances in the fabrication of EOIMs (based on an annealed proton exchange process patented by United Technologies Photonics, Inc.) have produced EOIMs that are extremely stable for optical power of up to a few hundred milliwatts. These modulators are based on the electro-optic or Pockel's effect, in which the index of refraction of the crystal varies with an applied field. Crystals such as $LiNbO_3$ or $LiTaO_3$ have high electro-optic coefficients; consequently, they require low driving voltages. These crystals have small loss tangents at rf frequencies, and are not as hydroscopic as earlier devices.

The fiber-optic link implemented by Interscience, Inc., under the Phase I SBIR effort, is based on the operation of a state-of-the-art $LiNbO_3$ EOIM manufactured by New Focus, Inc. A schematic representation of the proposed analog fiber-optic link is shown in figure 1.

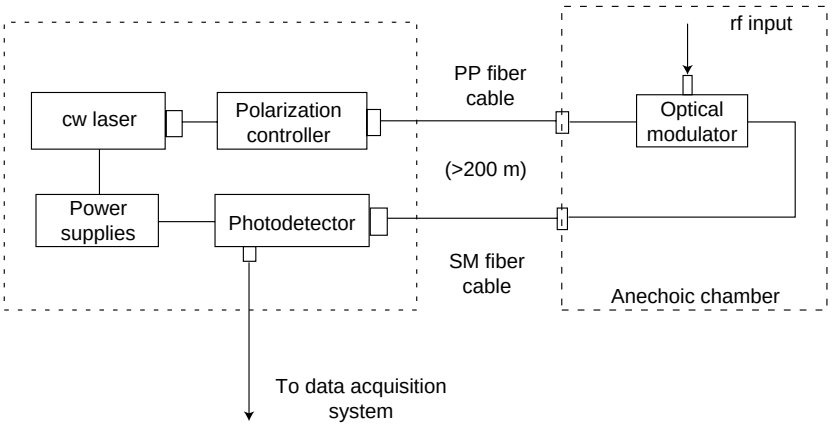

Figure 1. Schematic of externally modulated link measurement system layout.

2. Characteristics of the Mach-Zehnder Interferometer

The New Focus EOIM (model 4503) is a guided-wave Mach-Zehnder interferometer. As illustrated in figure 2, the interferometer consists of a single-mode input waveguide that is split into two separate single-mode waveguides separated by 40 mm. After a suitable length, the waveguides are recombined into a single-mode output waveguide. Electrodes are deposited along each waveguide arm, and are configured so that an applied modulation signal is a traveling wave predominantly in the transverse electric mode (quasi TEM) [1,2]. If the optical and rf field velocities are equal, there is no theoretical rf bandwidth limitation [3]. In practice, however, the bandwidth is limited by velocity mismatch and rf losses.

The application of an electrical signal to the input of the modulator rf section results in induced electric fields of opposite polarity across the two arms of the interferometer. The effect of this change is to retard the phase of the light in one arm, with respect to the light in the second arm. If the light in both arms are in phase, the interferometer has maximum output; if the phase is shifted by 180°, the interferometer has minimum output.

In general, the output light intensity, I_{out}(W), is related to the applied input signal V_{in}(V) by the expression

$$I_{out} = I_{in} \cos^2 \left[\frac{\pi^* V_{in}}{2 V_\pi} + \Phi_o \right], \quad (1)$$

where I_{in} is the input light intensity, Φ_o is any intrinsic or extrinsic static phase bias present on the interferometer, and V_π is the voltage required to cause a 180° phase shift between the two arms (i.e., to turn the modulator from fully on to fully off). The ability to adjust the static phase (Φ_o) of the modulator by changing the bias voltage has proven to be extremely important in reducing the harmonic content introduced by the modulator's nonlinear transfer function, achieving linear operation of the device within a bounded range of applied signals. For small signals, the modulator will operate in a linear fashion if Φ_o in equation (1) is set to $\pi/4$.

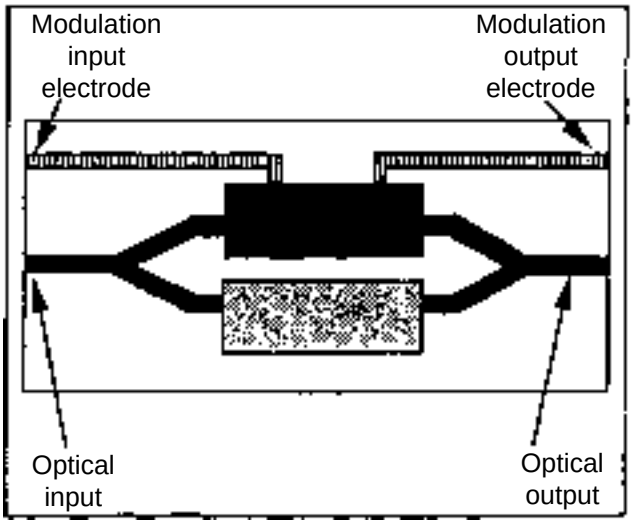

Figure 2. Typical Mach-Zehnder interferometer modulator layout.

The modulator's transfer function (ratio of the output to input power) can be defined as

$$\frac{P_{\text{out}}}{P_{\text{in}}} = \frac{1}{2}\left[1 + \cos\left(\frac{\pi * V_{\text{in}}}{V_{\pi}} + \frac{\pi}{2}\right)\right], \tag{2}$$

which is a nonlinear function of the input voltage V_{in}. It is important to point out that, when the modulator is biased at the $\pi/2$ point, the output will be approximately linear, depending on the input voltage. Distortion is expected for large rf signals on the order of $V_{\pi}/2$. Figure 3 shows the transfer function of a modulator biased with a 90° phase shift to allow full bipolar excursion of the input voltage with the optical power modulated from zero to its maximum value.

For the New Focus 4503 modulator, the drive voltage V_{π} is about 10 V dc; therefore, the transmitted optical power swings from its maximum, V_{in} = –5 V, to its minimum, V_{in} = +5 V, when biased at 90°. The advantage of the 90° bias is that second harmonics are eliminated and only the fundamental and odd harmonics of the signal spectrum are generated. For small signals, the response will be approximately linear.

3. Integrating the Modulator and Photodetector

Integrating a photodiode with the modulator, the voltage gain of the system (G_{mod}) can be expressed as the ratio of the output voltage of the photodiode V_{out} to the input voltage V_{in} of the modulator, as in the following equation:

$$G_{\text{mod}} = 20\log\left(\frac{V_{\text{out}}}{V_{\text{in}}}\right) = 20\log\left[\frac{Z_l * R_{ph} * \eta * P_{\text{out}}}{V_{\text{in}}}\right], \tag{3}$$

where Z_l is the impedance of the photodiode load (50 Ω), R_{ph} is the responsivity of the photodiode, and η is the resulting optical efficiency of the modulator/photodiode system due to insertion losses associated with

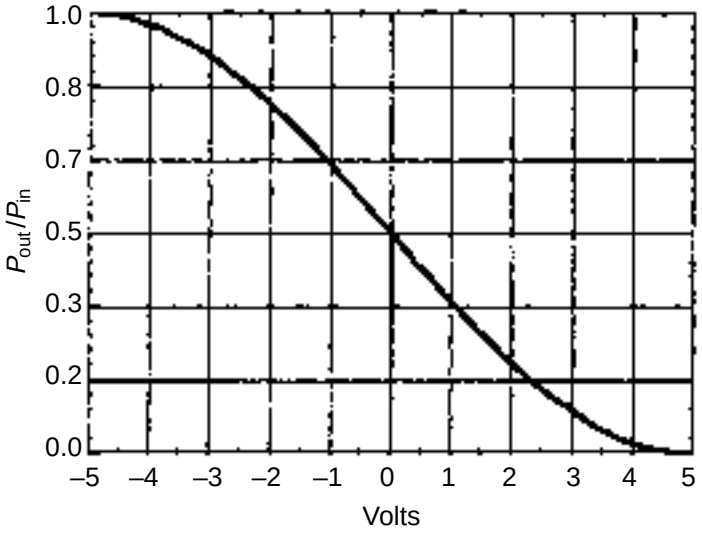

Figure 3. Transfer function of Mach-Zehnder modulator biased for a 90° phase shift.

the modulator, fiber-optic cable, and optical couplers. For the New Focus modulator and fibers used in this effort, the optical efficiency η was approximately 0.25. The responsivity (R_{ph}) for the HP83440C PIN photodiode selected for this effort was 0.8 W/A for ac signals.

Since P_{out} is related to the input optical power via equation (2), it is clear that the modulator-detector gain is a function of the laser power level injected into the modulator. Figure 4 illustrates the gain of the modulator-detector system calculated from equations (2) and (3) for two different values of the laser power. The driving voltages are shown from –5 V to +5 V, covering maximum signal excursions. The nonlinear behavior of the modulator caused large variations of the gain as a function of the driving ac voltage. The gain for extremely large signals (i.e., ±5 V) was about 4 dB lower than the gain for small signals in the millivolt range. The graph in figure 4 also shows the enhancement effect on the gain of the modulator due to higher laser power.

For a perfectly biased modulator, it can be shown that the modulation index (defined as $ß = \pi V_{in}/2V_{\pi}$) should be smaller than 0.552 radians to achieve a 1-dB output power compression point within the linear region of the device. This is equivalent to operating the device at approximately ±3.5 V, or 70 percent of V_{π}, which is around the bias point.

4. Determining the Minimum Detectable Signal of the Modulator/Detector

The sensitivity of the integrated modulator/detector system is dominated by the thermal noise of the photodiode's load, which corresponds to the combination of the diode shunt resistance and the input impedance of a post-amplifier stage. We selected a 50-Ω amplifier to obtain a large bandwidth for the receiver. The tradeoff in optimizing bandwidth is that the

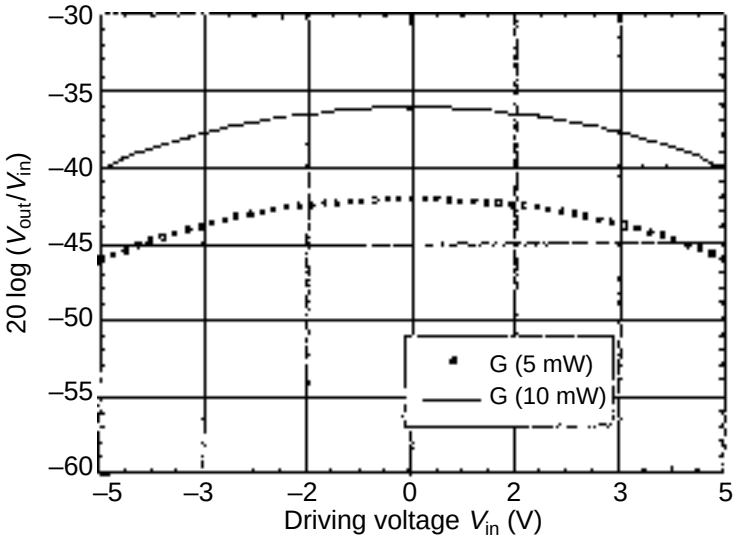

Figure 4. Modulator gain of integrated New Focus and HP8344OC photodiode.

low load impedance increases the thermal noise generated at the receiver. The peak noise current $(I_{\text{noise}})_{\text{peak}}$ can be determined from the expression

$$\left(I_{\text{noise}}\right)_{\text{peak}} = 6qB_n\left(I_{\text{dark}} + \frac{2kT}{q\,R_l}\right) , \tag{4}$$

where B_n is the noise equivalent bandwidth, I_{dark} is the dark current of the photodiode, $k = 1.38 \times 10^{-23}$ W/Hz is Boltzmann's constant, T is the absolute temperature of the device, and R_l is the load resistance (50 Ω).

The noise-equivalent bandwidth is different from the signal bandwidth, B_s, which is defined as the –3 dB frequency of the system-transfer function for a unit pulse. B_n is determined by approximating the area under the system-transfer function by a rectangle of equal area whose height is the maximum gain of the transfer curve (i.e., by requiring that $G_{\text{signal}} \times B_s = G_{\text{noise}} \times B_n$). The width of this rectangle defines the noise-equivalent bandwidth [4]. A practical result for a system with one pole is

$$B_n = \pi\frac{B_s}{2} . \tag{5}$$

This formula is also used for Gaussian low-pass filters and first-order resonant filters.

The corresponding signal bandwidth of the receiver can be calculated from the expression

$$B_s \approx \frac{0.35}{t_r} . \tag{6}$$

The receiver's risetime is determined by the approximation

$$t_r \approx 2.2\,R_l * C_t , \tag{7}$$

where $C_t = C_j + C_{\text{case}}$ is the terminal capacitance made up of the parallel combination of the junction capacitance, C_j, and the packaging or case capacitance, C_{case}.

The noise bandwidth is approximately 7.5 GHz, based on the expected signal bandwidth B_s of 5 GHz (eq (5)). The resulting peak noise current (eq (4)) is approximately 6.8 μA at the receiver load (at room temperature). For a 50-Ω load, this is equivalent to a 340-μV noise peak voltage (–57 dBm (electrical)).

The receiver noise is often expressed in terms of noise-equivalent optical power (NEP = I_{noise}/R_{ph}), which is a measurement of the smallest detectable optical power for the given bandwidth. The NEP peak value in this case is about 8.5 μW (optical) (i.e., –21 dBm (optical)).

5. Determining the Maximum Laser Power Required for the Fiber-Optic Link

Since the link must maintain a dynamic range of 40 dB for a measured rf signal and the minimum detector signal is –57 dBm (electrical), the maximum expected output signal from the photodetector is –17 dBm, which, in turn, corresponds to a maximum current of 0.6 mA into a 50-Ω load. The expected maximum optical power at the detector is, therefore, 0.75 mW optical, which corresponds to approximately 3 mW of maximum optical power at the modulator input due to the 25-percent optical efficiency of the modulator. This range of optical power is valid for devices that operate in their linear regions, as well as on single polarity signals. Due to the characteristics of the transfer function of the modulator (shown in fig. 3), the required maximum optical power must be increased to 8 mW to account for bipolar signals. The actual maximum power of the laser will be much higher to ensure that signals will stay within the linear region of the device, and to compensate for additional optical power losses in the polarization-controller unit and the multiple optical connections through the link. We estimate that these additional losses could reach up to 10 percent of the laser's output power.

If the modulator is operated up to its 1-dB compression point ($V_{in} = \pm 3.5$ V, or 70 percent of V_π around the bias point), a minimum laser power of about 13 mW will be required to measure bipolar signals covering a dynamic range of 40 dB from a tangential noise of –57 dBm at the receiver.

6. General Characteristics of the Integrated Fiber-Optic Link

To design a practical fiber-optic link using the modulator and photodetector described in the previous sections, it will be necessary to add preamplification and postamplification stages. As we discussed in section 5, the modulator/detector can be expected to transmit measured signals ranging from –17 to –57 dBm at the photodetector's output. If we estimate the electrical loss of the modulator/detector to be ≈40 dB (see fig. 4), we can infer that, to maintain this output signal range, input signals must range between 23.6 dBm (340 mV) to –16.4 dBm (34 mV). To meet the original minimum detectable signal specification discussed in the introduction, it will be necessary to provide at least 51 dB of preamplification to the modulator. The range of expected voltages and power levels at each node of the integrated link (fig. 5) are shown in table 1. We estimated the values in this table under the assumption that the linear approximation model holds.

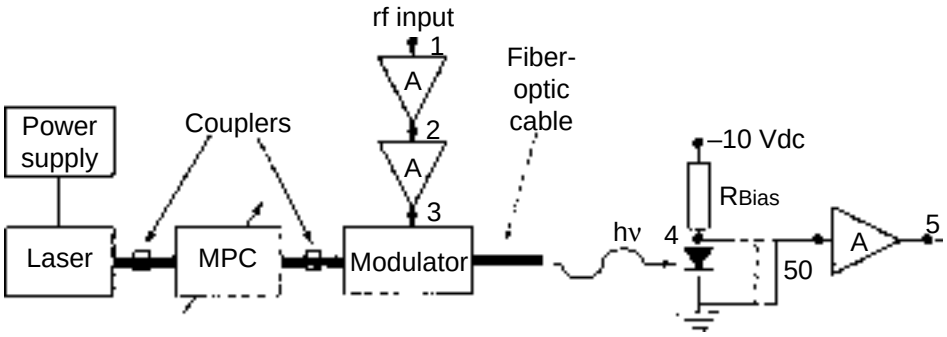

Figure 5. Schematic of the modulator and detector system, with numbered nodes.

Table 1. Range of expected voltage/ power levels for each node of integrated link.

	Node number			
Power/voltage	1	2	3	4
P_{max} (dBm)	–25	–1*	23*	–17
P_{min} (dBm)	–65*	–41	–17	–57*
V_{max} (mV)	12.5	200	3160	31.6
V_{min} (mV)	0.12	2	1.6	0.34

**Critical design value*

The major design constraints for the integrated fiber-optic link are driven by the following factors:

(a) The thermal noise level of the detector load (–57 dBm);

(b) The saturation level of the last-stage amplifier (at least 24 dBm); and

(c) The minimum noise figure of the amplifiers that conditions the signal to drive the modulator. The minimum output signal at tangential noise must be ≥16 dBm.

Design considerations used for the calculations in table 1 include the following measurements:

Amplifier gain G_A = 24 dB,
Modulator-detector loss = G_{MD} 40 dB,

where

G_{MD} = 20 log | $V4/V3$ | (dB),
P_1 (1-dB compression point) = + 24 dBm,
Bandwidth = 5 GHz.

In selecting the amplification stages to condition the rf signals that drive the modulator, we decided to use amplifiers with a bandwidth greater than 5 GHz, which allowed us to test the capabilities of the integrated modulator link to operate at frequencies up to 10 GHz.

We followed a systematic approach to characterize the responses of the various components of the external modulator-based optical link. Specifically, we took measurements of the frequency responses and pulse responses of the components under different operating conditions.

7. Performance of the Modulator and the Photodiode

A photograph of the New Focus Model 4503 modulator used for our work is shown in figure 6. This device is about $40 \times 20 \times 15$ mm in size, without the rf and bias connectors. The dc bias voltage is applied through the top connector, with no need for external bias circuitry. The rf input is shown at the bottom of the device, and the pigtailed optical fibers are seen at the input and output areas of the module. The input fiber is a polarization-maintenance fiber that preserves the polarization of the laser light as it enters the modulator's optical guide. The output cable is a single-mode 9/125-μm fiber. Both input and output fiber-optic cables are terminated in ST connectors so that they can be coupled directly to the continuous wave (cw) source of laser light and to the photodiode receiver.

The design of this type of modulator has been optimized to operate with a laser light wavelength of 1.3 μm. The frequency response of the modulator was measured at New Focus, Inc., using a Hewlett Packard (HP) 40-GHz lightwave optical analyzer (fig. 7). We observed the –3-dB bandwidth to be 10.5 GHz. We obtained a combined modulator/detector gain of –65.3 dB for a particular value of the optical laser power, which can be improved by increasing the laser power. The flatness of the frequency response curve was within ±1 dB.

The receiver that we used was a HP PIN photodiode model HP83440C, which was coupled directly to the modulator output fiber. A picture of this device is shown in figure 8. The fiber-optic cable is connected directly to the network analyzer port, with a –10-V inverse dc bias provided through the top cable. We also measured the frequency response of this photodiode by a calibrated laser diode source at HP; the result of this measurement is shown in figure 9. From this plot, we observed that the –3-dB bandwidth of the device was 18 GHz, with less than a 1-dB drop at 10 GHz. The maximum detector dark current was measured at 10 nA, which is a much smaller unit than the thermal noise current, estimated to be 6.8 μA, from equation (4).

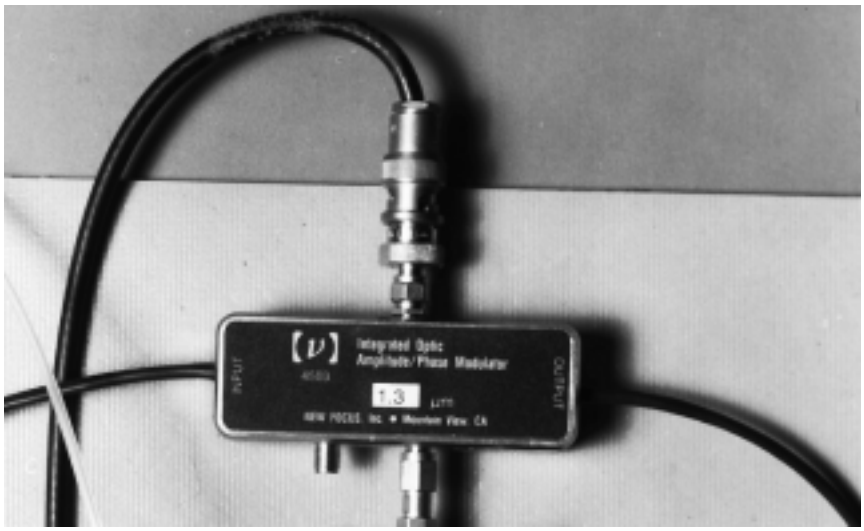

Figure 6. Photograph of New Focus Model 4503 $LiNbO_3$ modulator.

Figure 7. Frequency response of New Focus Model 4503 measured by the factory (3 dB/div vertical scale).

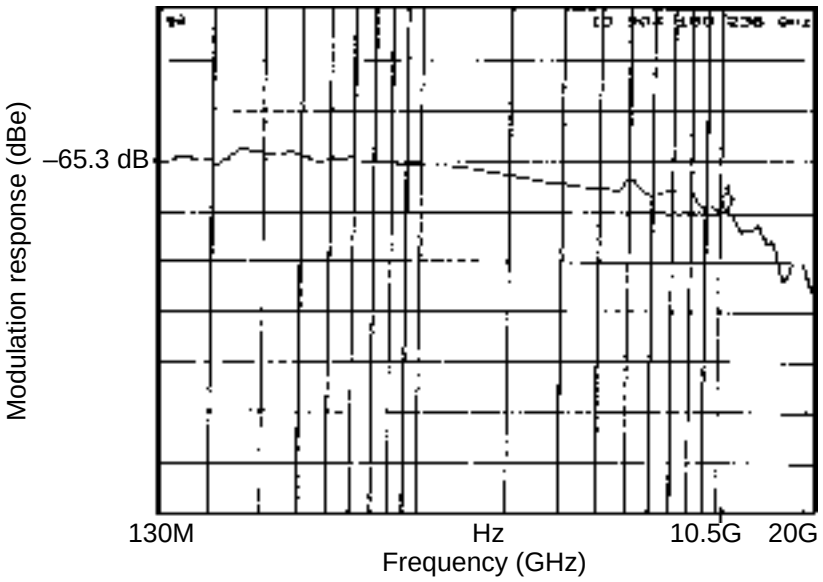

Figure 8. Photo of HP PIN photodiode receiver.

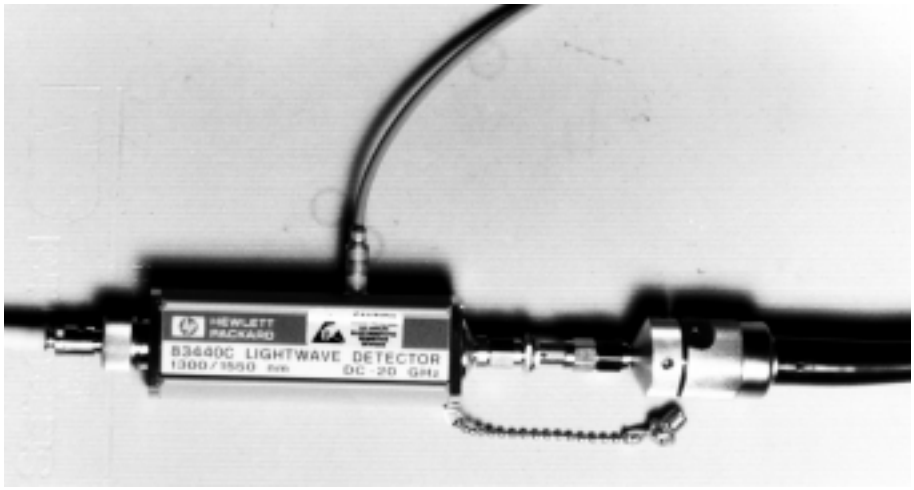

Figure 9. Frequency response of the HP PIN photodiode receiver.

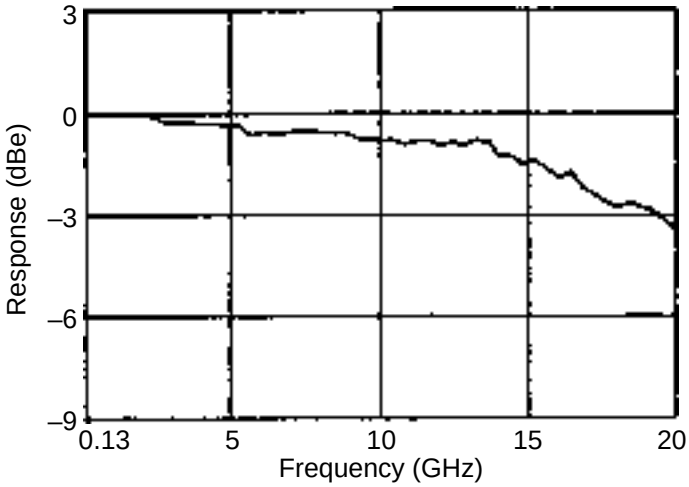

Based on the performance of this modulator and the HP photodiode, it is possible to consider extending the bandwidth of the initially specified optical link to beyond 5 GHz. Our analysis of the specifications that can be realized using such a broadband system will be discussed later in this report; however, we anticipate that the noise bandwidth will be much larger, which will directly affect the sensitivity and dynamic range that can be obtained with the extended bandwidth system.

8. Performance of the Amplifiers

The first amplifier that we investigated was the B&H model AC9011H20, a 50-Ω device with a bandwidth from 10 kHz to 9 GHz, a gain of 20 dB ±1.2 dB, 1-dB compression of 20 dBm, and a noise figure of 5.5 dB at 9 GHz. This noise figure implies an expected minimum input noise power level of –72 dBm (56 μV), with a 5-GHz bandwidth (or noise power) of –69 dBm (80 μV) at a 10-GHz bandwidth, assuming the worst-case noise figure of 5.5 dB for frequencies lower than 9 GHz. We measured the output power of this amplifier at the 1-dB output compression point at 24 dBm, which corresponds to the dynamic range of 72 dB measured from the root mean square (rms) noise level at the output to the 1-dB compression point. The B&H amplifier requires a double-sided power supply consisting of a 24-V_{dc} supply with a 330-mA current draw, and a –5-V_{dc} supply with a –24-mA draw.

The second amplifier that we evaluated for this effort was a Model SHF79B 50-Ω broadband amplifier designed by a German company, SHF Design (SHF). The frequency response of the SHF amplifier spans from 20 kHz to 10 GHz, with a gain of 25 ±1 dB, a risetime shorter than 35 ps, and a noise figure (nf) of less than 6 dB. The output power of the amplifier at a 1-dB compression point is 10 dBm. The SHF amplifier requires a single power supply of 15 to 20 V_{dc}, with a current supply of only 130 mA. This lower power supply requirement makes it more attractive for use in a battery-operated device, when compared to the B&H amplifier. The limitation of the SHF amplifier is that its output power at the 1-dB compression point is only 10 dBm, compared to approximately 24 dBm for the B&H amplifier. The physical dimensions of the SHF amplifier are similar to the B&H amplifier (i.e., $70 \times 50 \times 25$ mm).

Figures 10a and 10b show the high- and low-frequency responses of the B&H amplifier module. The gain was approximately 20 dB, with a low-frequency cutoff of ≈10 kHz and a high-frequency cutoff at 9.6 GHz. (We obtained this measurement with an HP8510C automatic network analyzer.)

Similarly, figure 11 shows the frequency response and the nf of the SHF79B amplifier measured by SHF Design. The nf was ~6 dB for frequencies below 5 GHz, dropping down to the 4- to 5-dB range at higher frequencies. The gain was about 25 dB within a ±1-dB tolerance, and the bandwidth was very close to 10 GHz.

Figure 10. Responses of the B&H amplifier: (a) low-frequency and (b) high-frequency.

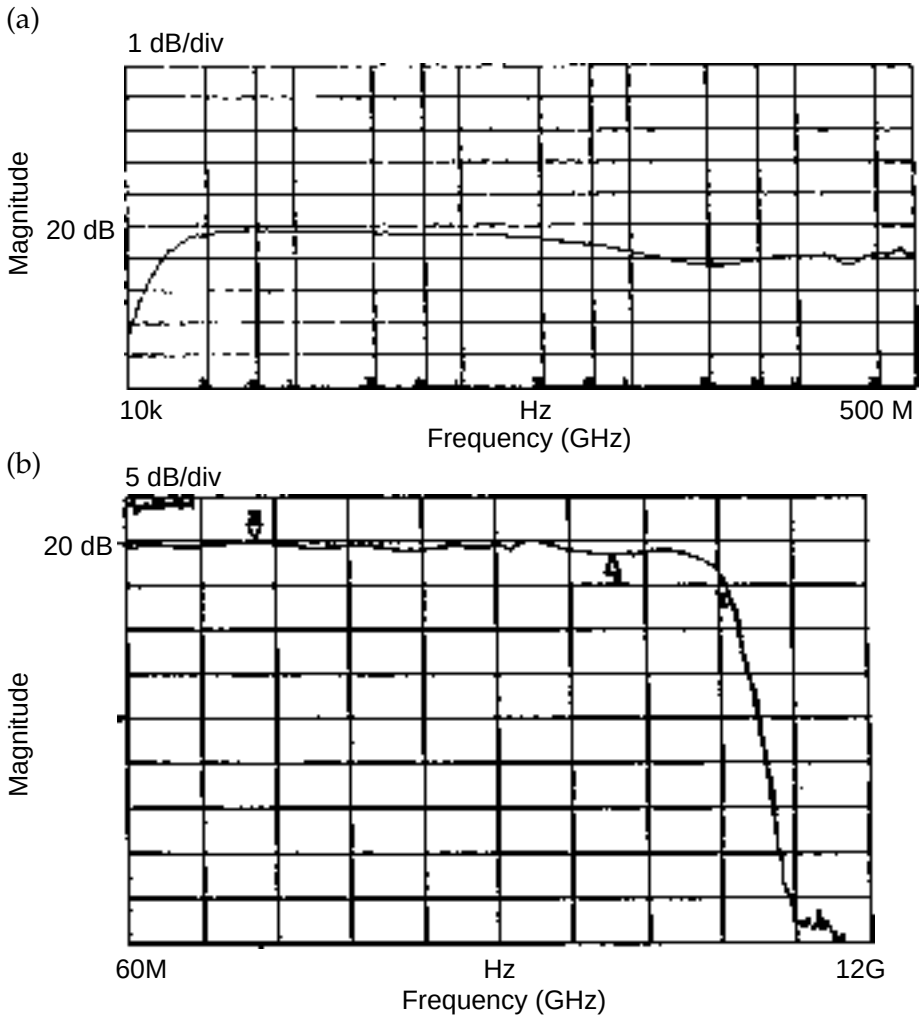

Figure 11. Frequency response of the SHF79B amplifier.

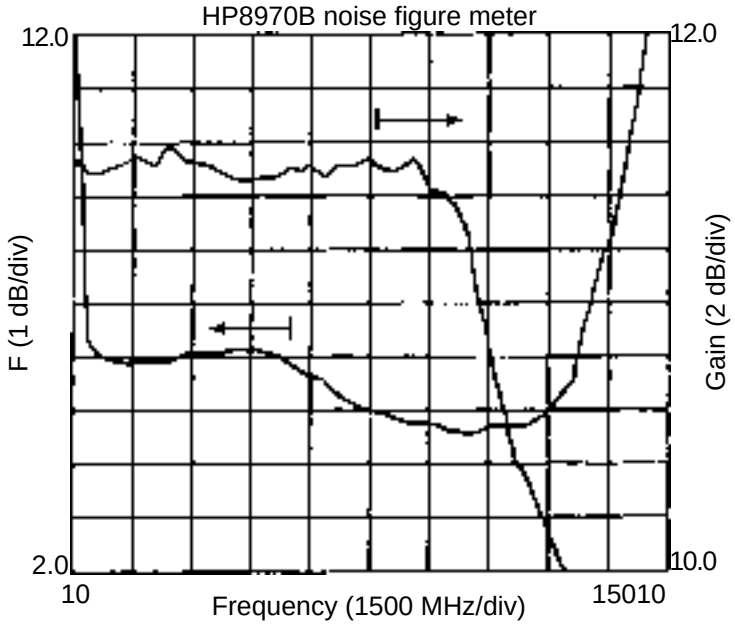

Rauschmaβ, noise figure (NF):<6 dB,
Verstärkung, gain: 25 dB

9. CW Laser Description

The test setup of the integrated system includes the basic components shown in the diagram in figure 1. The laser is a high-powered diode-pumped solid-state laser, based on a Nd:YAG crystal (neodymium: yttrium aluminum garnet) operated in cw mode. The laser output has a single transverse TM_{00} mode structure, and the laser is linearly polarized. The relative intensity noise (rin) measured at frequencies between 10 MHz and 18 GHz is more than –165 dBm/Hz, with a line width less than 5 kHz. The laser has a pigtailed output fiber of the single-mode 9/125-µm type that terminates in an ST connector.

Figure 12 shows the Amoco microlaser model Whisper 1320-105/w18 that produces approximately 9 mW of optical power. The output is a single spectral line centered at 1319 nm. This emission line has a spectral width of about 0.3 nm and contains approximately four longitudinal axial modes. Each longitudinal mode is extremely narrow, with an approximate width of 5 Hz. Figure 13 shows a diagram of the spectral composition of the single-mode structure.

Since the modulator input requires a specific linearly polarized light, it was necessary to adjust the polarization plane of the laser light at the end of the pigtailed fiber. To accomplish this, we used a HP manual polarization controller (MPC) Model MPC1000. The MPC1000 is a precision component that manually controls the polarization of the light in the optical fiber. The MPC1000 was designed to transform any input polarization state to any output polarization state in the 850-, 1300-, and 1550-nm wavelength windows. It introduces negligible optical insertion loss, even at longer wavelengths, and is especially useful in systems in which a transformation between two static polarization states is required. This device is used to modify the polarization state for amplitude and phase modulators, and to match the polarization states in the two arms of an optical fiber interferometer.

Figure 12. Amoco laser source, including pigtailed single-mode fiber.

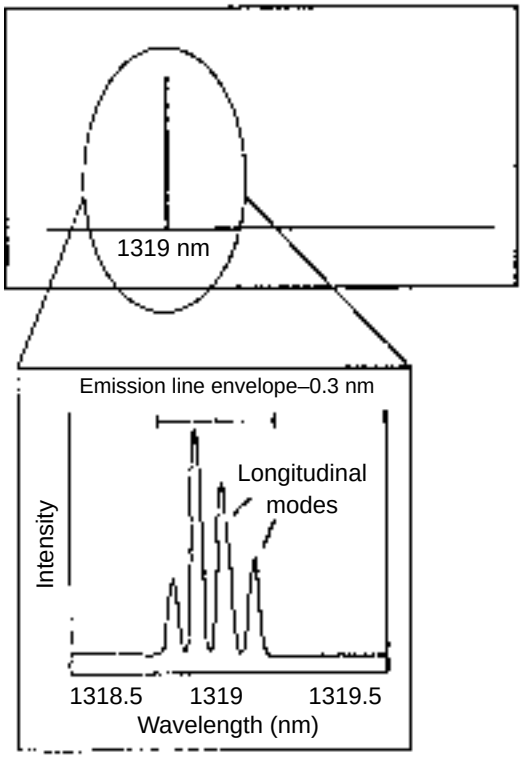

Figure 13. Spectral structure of the 1.3-μm single-mode laser output.

The procedure that we used to set up the MPC1000 consisted of winding the single-mode fiber in loops around the discs of the device to produce a fiber analog of a bulk optic-rotatable fractional waveplate. Input light polarization can be transformed to any output state of polarization simply by adjusting the relative angles between the three discs. When single-mode fiber is wound onto a disk of the MPC1000, it is equivalent to a fractional waveplate with a retardation angle Φ (in radians), given by

$$\Phi = 0.015\, m\pi \frac{d^2}{\lambda} \ , \tag{8}$$

where λ is the wavelength of the light in nanometers, d is the diameter of the fiber cladding in micrometers, and m is the number of fiber loops on the discs [5]. The optimum combination of waveplates for polarization transformations is three quarter-waveplates, so that $\Phi = \pi/2$ (although values of Φ between $\pi/3$ and $2\pi/3$ will provide satisfactory operation). In the case of a 125-μm diameter fiber and a λ of 1300 nm, the configuration recommended is for three loops on each disc. Figure 14 shows the result of this calculation for the 125-μm cladding diameter fiber. Depending on the misalignment angle between the laser output of the Amoco laser and the polarization plane required for the light at the modulator input fiber, it is possible to find the optimum range of angles by changing the number of loops per disc. Figure 15 shows the top view of the MPC1000 that we used for this work. This device is approximately 30 cm long × 10 cm high. We terminated the single-mode fiber on both ends with ST connectors.

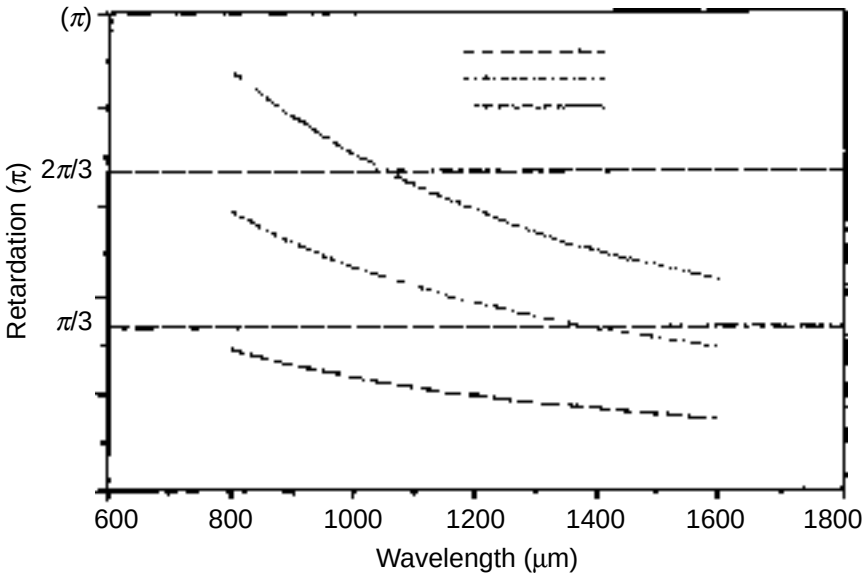

Figure 14. Retardation angle (Φ) for the MPC1000 manual polarization controller.

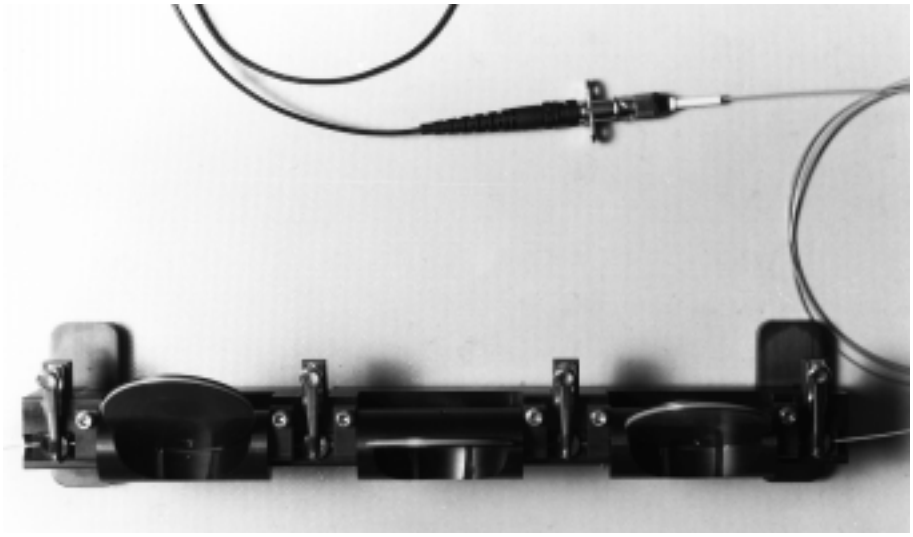

Figure 15. Top view of the MPC1000 polarization controller with three turns per disc.

10. Integrating the Fiber-Optic Link

To determine the compatibility and performance of the integrated fiber-optic link, we arranged the individual components with a single amplification stage at the modulator's rf input (fig. 5). The modulator was biased at $V_{\pi/2}$ = +10 V_{dc} to set its transfer function at its quadrature or half-maximum intensity point. The bias current is negligible, since the equivalent circuit is primarily capacitive and is almost an open circuit at dc, except for some minute leakage current. With no rf signal applied to the modulator, the polarization state of the light coupled to the modulator input is adjusted by moving the MPC's discs. An optimum polarization match is achieved when the dc voltage of the photodiode at node 4 in figure 5 is maximized. (Alternatively, the photodiode was replaced by a calibrated Newport optical power meter to measure the maximum power

transmitted through the modulator, after matching the polarization stage. From this measurement, we estimated that the modulator and its connectors contribute 6 dB of loss, which is in close agreement with the manufacturer's specifications.)

The polarization controller's discs are then locked into position. The mechanical stability of the polarization controller is acceptable for laboratory or experimental prototype tests, and no further adjustments are required during operation of the link. However, when it was moved accidentally, a short (5-cm) fiber-optic cable left free at the end of the polarization controller caused the optical power to vary. This variation was due to the fact that the fiber used in the polarization controller should have been a regular single-mode (i.e., a nonpolarization-maintaining) fiber. The polarization state in this piece of cable can be changed by twisting or stretching the fiber at the exit of the polarization-controller device. A simple solution to this problem is to mount the ST connector of the single-mode fiber rigidly to the polarizer's body.

11. Frequency Response of the Integrated Fiber-Optic Link

Figure 16 is a picture of the complete system setup, with a single amplifier at the modulator input. We used two automatic network analyzers to measure the frequency spectrum from 10 kHz to 12 GHz. We kept the laser power fixed for most of the experiment, except to check the gain of the system versus the input power by causing a slight mismatch of the polarization state at the polarization controller that reduced the optical power launched into the modulator. Figure 17 is a closeup picture of the SHF amplifier connected to the modulator.

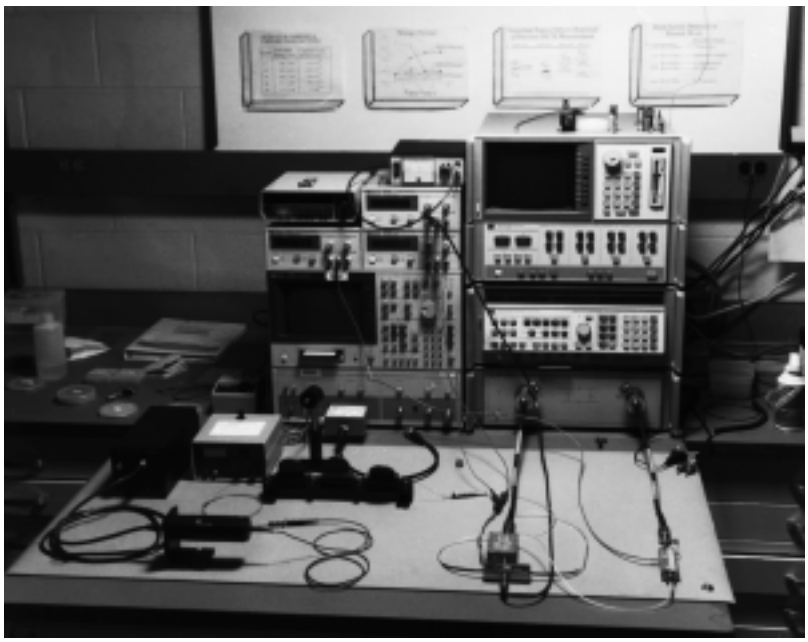

Figure 16. Test setup of the integrated optical link.

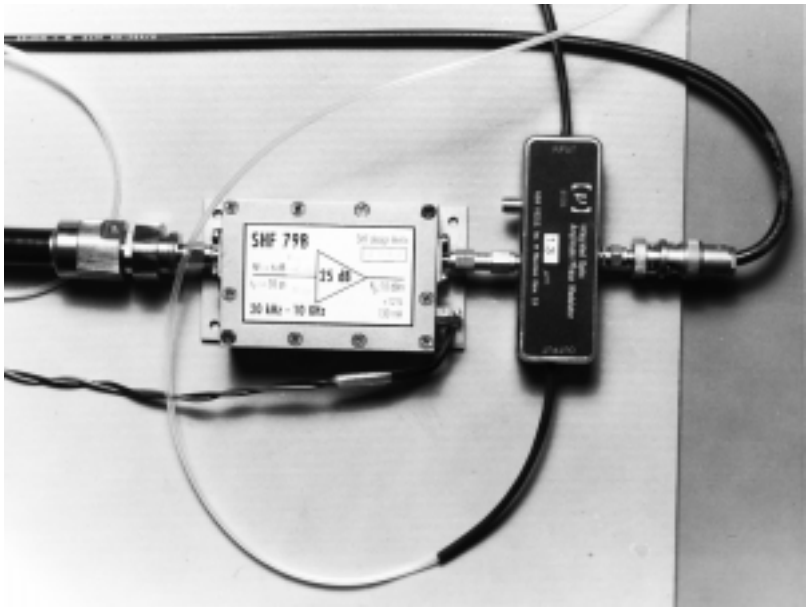

Figure 17. Closeup photograph of amplifier and modulator.

11.1 Frequency Response Using the B&H Amplifier

Figure 18 shows the 10-kHz to 500-MHz frequency responses for the integrated fiber-optic link, using the B&H amplifier to drive the modulator. Accounting for the gain of the amplifier, we measured the gain of the modulator/detector (G_{MD}) to be ≈ –42 dB. This is the estimated gain for a modulator bias voltage (applied at the dc port) of $V_{\pi/2}$ = +10 V_{dc} and for an optical power of approximately 1.5 mW at the detector. The –3-dB low-frequency cutoff is near 10 kHz in this case. The flatness of the link gain is within 1 dB.

Similarly, we measured the high-frequency response of the link by using the HP8510C automatic network analyzer (ANA). In this case, we attenuated the signal by 24 dB to compensate for the amplifier gain. The gain plot shown in figure 19 corresponds to the complete link response. The modulator/detector loss (G_{MD}) was ~42 dB. The frequency band extended up to 6.1 GHz, although there was a significant drop in gain from 60 MHz to 1.7 GHz; this drop could be due to a possible mismatch of impedance between the amplifier output and the modulator. For frequencies beyond 8.2 GHz, the response drops drastically, indicating a low-order pole configuration of the B&H amplifier. This response is in agreement with the amplifier response shown in figure 10b.

11.2 Frequency Response Using the SHF79B Amplifier

With the same equipment and under similar operating conditions, we performed tests on the frequency response of the integrated link using the SHF79B amplifier for the modulator and detector. Figure 20 shows the frequency response of this link in the frequency range from 10 kHz to 500 MHz. The low-frequency cutoff is approximately 20 kHz, and the gain of the modulator/detector system is near –42 dB. The frequency response falloff is smoother than that obtained for the link with the B&H amplifier, because the SHF amplifier has a wider bandwidth.

Figure 18. Frequency response of the integrated optical link with the B&H amplifier from 10 kHz to 500 MHz.

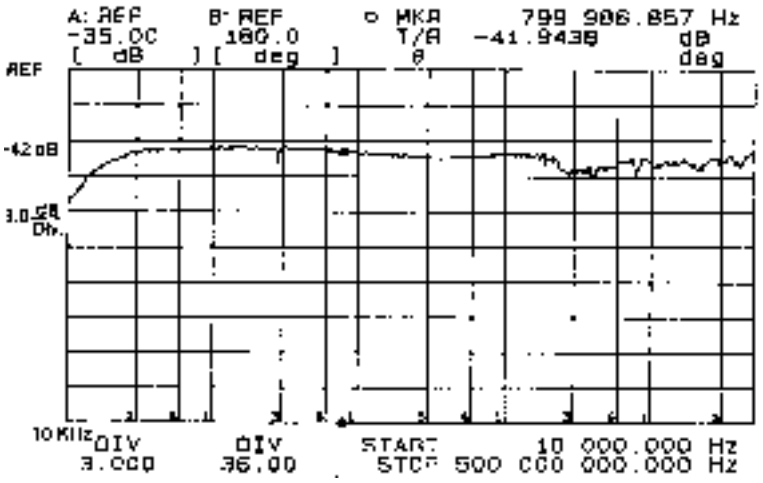

Figure 19. Frequency response of the link with the B&H amplifier from 0.06 to 12 GHz.

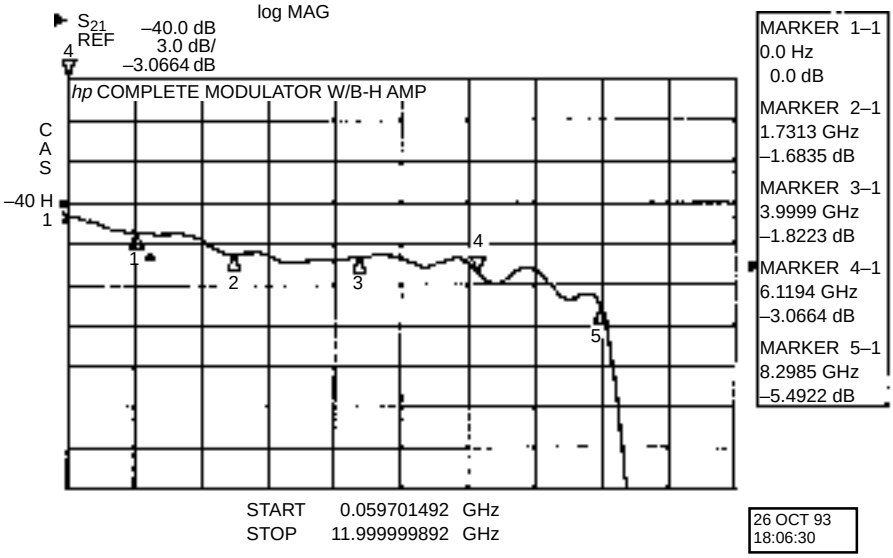

Figure 20. Frequency response of the integrated optical link with the B&H amplifier from 10 kHz to 500 MHz.

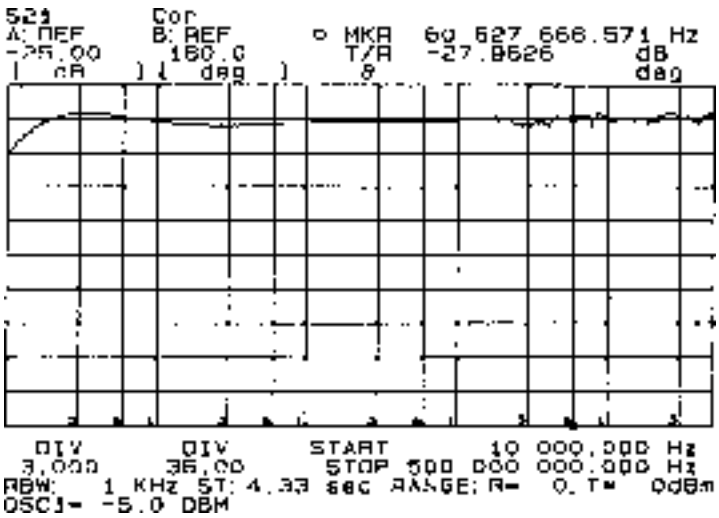

The ripple for frequencies higher than 30 MHz was about 1 dB larger than in the previous case. Figure 21 shows the high-frequency response noted when the ANA was scanned from 60 MHz to 12 GHz. The gain was near –42 dB and stayed reasonably flat up to 7.2 GHz, after which an oscillation similar to that in figure 19 was seen.

We believe that this oscillation was caused by an optical resonance. Reflections from a connector or coupler interface create standing waves that could affect both the laser or the photodetector, depending on whether the mismatch is on the input or output fiber. To determine if this reflection was on the output fiber, we inserted 100 m of single-mode fiber-optic cable between the exit of the modulator and the photodiode. Figure 22 shows the gain traced in both cases, with the short (1-m) pigtail fiber of the

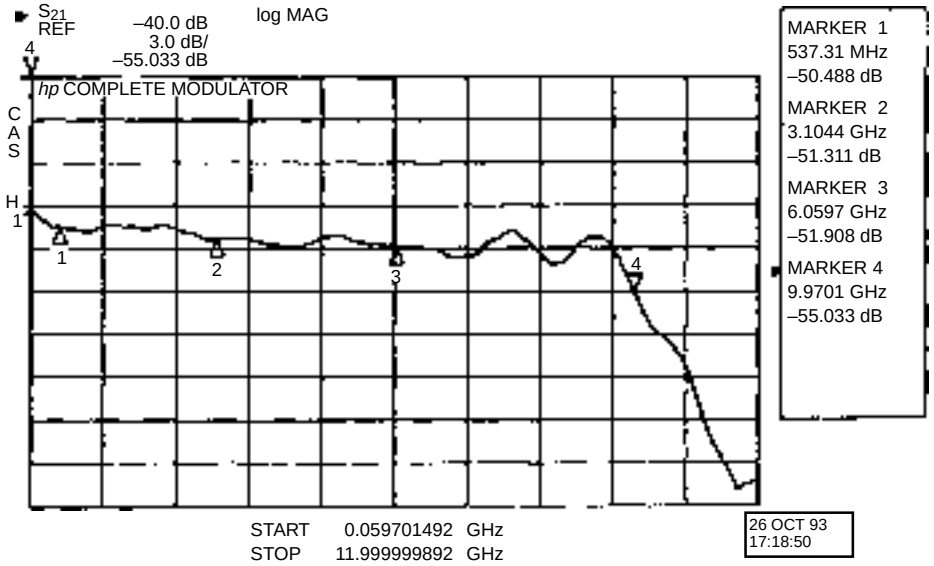

Figure 21. Frequency response of the link with the SHF79B amplifier from 60 MHz to 12 GHz.

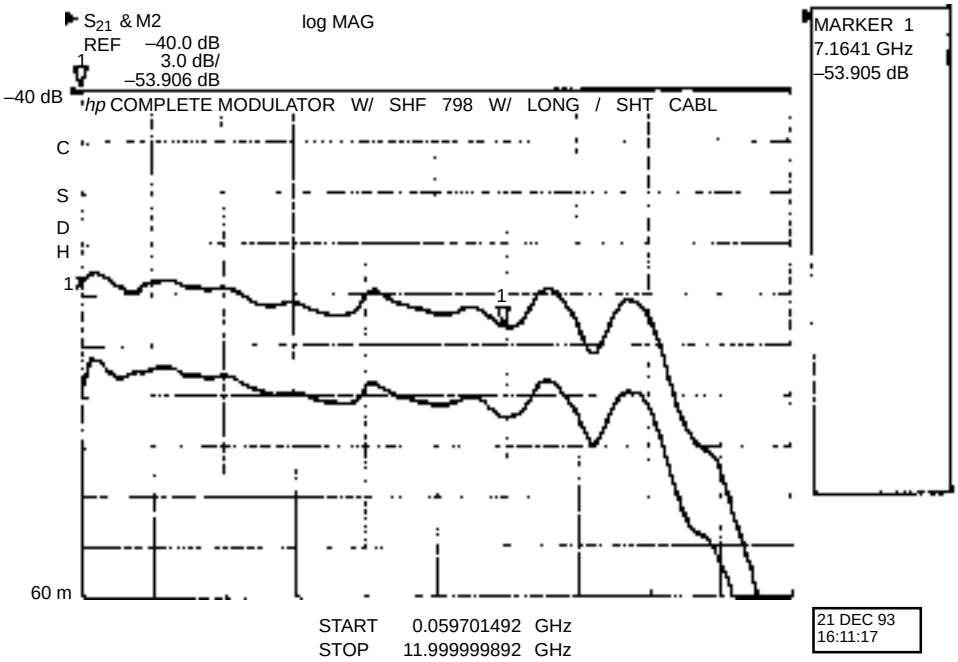

Figure 22. Frequency response of the link with 1 m of fiber-optic cable and with 100 m of cable after the modulator.

modulator and the 100 m additional cable as the upper and lower traces, respectively. There was ~4 dB of loss due to the optical cable losses and the affects of one additional coupler between the modulator output fiber and the detector. In both cases, the ripple stayed unchanged, indicating that possible reflections at the detector's end of the fiber-optic cable were not responsible for the oscillation.

We anticipate that the ripple effect at high frequencies can be significantly reduced or eliminated by using an optical isolator at the laser output—a standard practice to avoid spurious resonance. A fiber pigtailed optical isolator costs about $1K, and is available from sources such as E-TEK Dynamics, Inc., or Isowave, Inc. We did not investigate this issue further, because that type of isolator was not available for this project. Amoco, the laser manufacturer, sells lasers with an integrated optical isolator that provides 30 or 60 dB of isolation and can be factory-equipped with a polarization-maintaining input fiber pigtail and connector to maintain polarization without external control.

11.3 Modulator Performance Versus Bias Voltage

Equations (1) and (2) showed that changes in the bias voltage of a modulator can be considered as a phase shift of the modulator transfer function. Figure 23 shows the frequency response of the link with the SHF amplifier for bias voltages of 10, 8, and 6 V_{dc}, respectively; the relative shape of the curves remains unchanged. The gain dropped by approximately 1.5 dB when the bias voltage of the modulator was decreased from 10 V to 8 V; from 8 V to 6 V, the gain decreased by 3 dB. In the first case, this drop in bias voltage caused a phase shift of the transfer function of 18°, with respect to the quadrature point of the modulator. In the case of the 6-V bias voltage, the relative phase shift corresponds to 36°. The phase shift

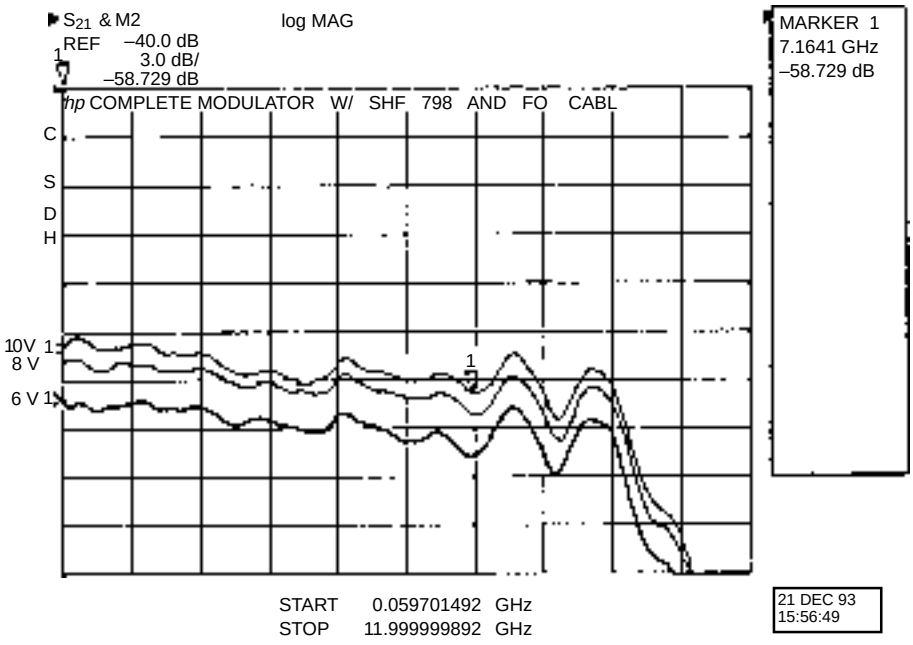

Figure 23. Frequency response of the complete link with the SHF amplifier modulator biased at 10, 8, and 6 V, respectively.

translated the transfer function away from the ideal quadrature point of operation of the modulator; therefore, the effective linear operating region, as well as the modulator gain, was reduced. This reduction, in turn, caused the cutoff or saturation of the output signal at smaller peak levels. For the 6-V_{dc} bias voltage case, this attenuation effect was more severe, since the nonlinear components of the modulator response tended to play a more significant role.

12. Time Domain Response

12.1 Pulse Response of the SHF Amplifier: Determining Tangential Noise Floor

From design considerations, the most critical factor in achieving the required sensitivity of the modulator link at the input stage of the system is the low noise performance of the first-stage amplifier. Figure 24 shows a diagram of our test setup for the sensitivity measurements of the SHF amplifier. We used a pulse generator (Model BNC8010, manufactured by Picosecond Pulse Labs (PPL)) to produce a rectangular pulse. We split the pulse using a 3-dB coupler—connecting one arm of the coupler directly to an oscilloscope trigger unit, and coupling the second arm to two sets of attenuators. Total attenuation was 68 dB, or 2512 times the voltage. The oscilloscope that we used was a Tektronix TDS640 with a 400-MHz bandwidth or, equivalently, a pulse risetime response of 0.9 ns. The pulse generator output, the attenuators, and the connectors were all 50-Ω devices, so that the characteristic impedance of the entire system was matched to reduce reflections and standing waves. Figure 25 shows the results of this measurement. The top trace, shown in segmented lines, corresponds to the input pulse measured in channel 2 of the scope. The bottom trace corresponds to the output signal of the amplifier, as measured in channel 1 of the scope. The peak of the square pulse of the output signal is at the tangential noise level, and is easily discernible. Based on this measurement, a minimum detectable output signal at the tangential noise level is about 1.5 mV, which corresponds to an input signal of 90 μV. The frequency band of this measurement is limited by the oscilloscope's bandwidth, which is 400 MHz. Extrapolating the signal level of 90 μV (measured with a bandwidth of 400 MHz) to a 5-GHz bandwidth, we estimated

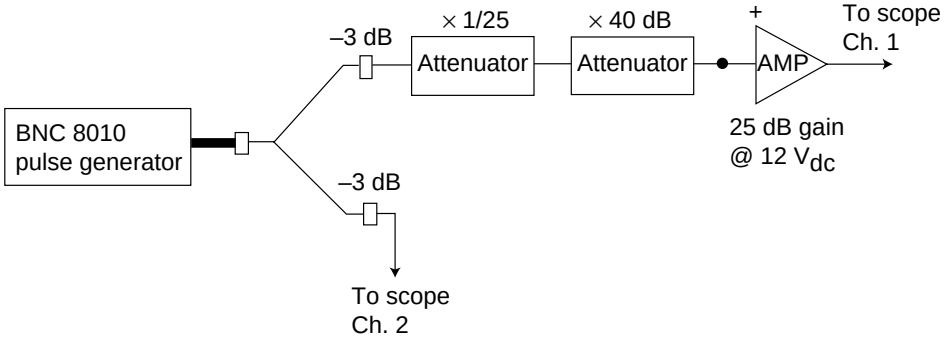

Figure 24. Test setup for time domain measurements of the SHF.

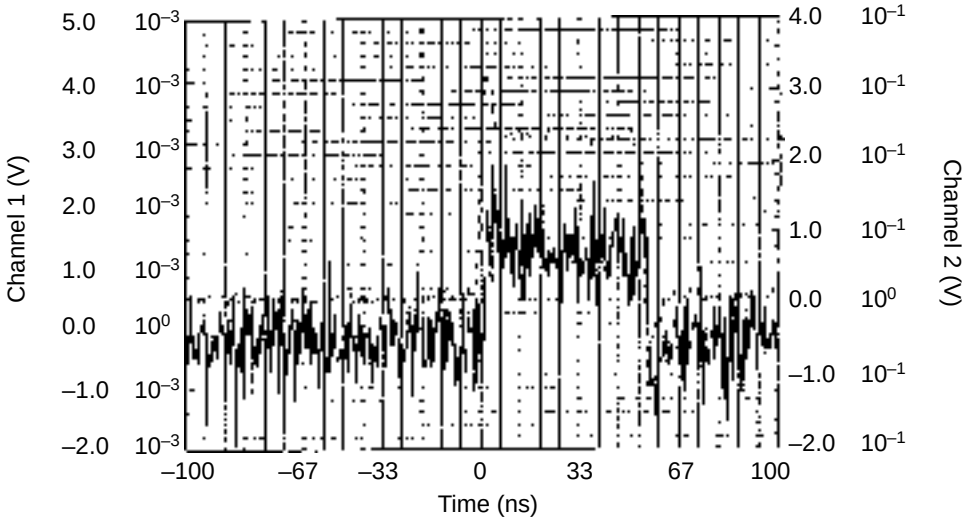

Figure 25. Pulse response of the SHF79B amplifier. (The upper trace (segmented line) is the input signal before attenuation; the lower trace (solid line) is the amplifier output signal.)

a minimum sensitivity of 318 μV. However, based on the amplifier's actual specifications, the tangential noise at the 5-GHz instantaneous bandwidth is expected to be at least 50-percent smaller than our estimated value. In principle, it is possible to reduce noise pickup due to both power supply fluctuations and bias electrical connections. Further improvements should be incorporated in a more-refined coupling and bias subsystem as part of the final link.

12.2 Pulse Response of the Modulator Link

Figure 26 shows the diagram of the test setup used to measure the time domain response of the integrated fiber-optic link using the SHF amplifier. We used a pulse generator (BNC 8010) to produce a rectangular pulse. We split this signal with a 3-dB coupler. We connected one arm of the coupler to the trigger unit and channel 2 of the TDS640 oscilloscope, and coupled the second arm through a 6-dB attenuator and the integrated link to a second oscilloscope channel. Figure 27 shows the result of this measurement. The lower trace, shown in segmented lines, corresponds to the input pulse to the attenuator measured by channel 2 of the oscilloscope. The upper trace corresponds to the output of the photodetector measured by channel 1 of the oscilloscope.

From the upper trace in figure 27, we observed that the square pulse signal at the detector's output was at the tangential noise level. This photodiode signal was 0.4 mV (i.e., –55 dBm), while the corresponding signal at the amplifier unit was 3.5 mV_{peak} (i.e., approximately –36 dBm), as determined from the lower trace. This implies that the modulator/detector loss was approximately 43 dB under these test conditions.

Several issues must be considered when comparing the results of this measurement with the design values of table 1. First, the measured noise level at the receiver load was 2 dB higher than the –57 dBm estimated in table 1. This was caused primarily by the laser noise transmitted through the modulator and detected by the photodiode. Additionally, the modulator/detector gain was about 3 dB lower than the estimates given.

Figure 26. Test setup for pulse measurements of the integrated link.

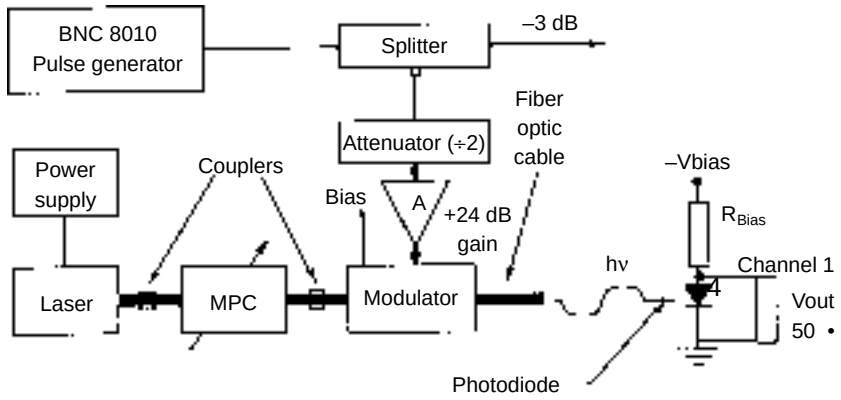

Figure 27. Pulse response of the modulator-based link with the SHF79B amplifier. (The lower trace (segmented line) is the input signal; the upper trace (solid line) is the output signal from the photodiode.)

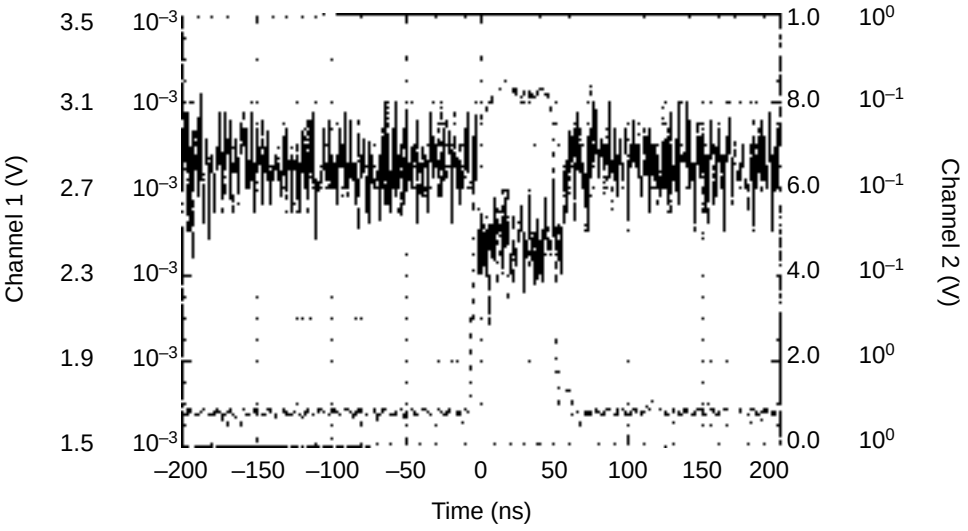

Both of these values combined to give a minimum detectable signal at the modulator's input of –12 dBm (i.e., ~55 mV), which is much higher than the 32 mV estimated in table 1. By bringing the gain G_{MD} up to –40 dB, it was possible to obtain –15 dBm (i.e., 40 mV) at the modulator input. To further reduce the noise level, the noise contribution from the laser source must be reduced through better control and stabilization of the Nd:YAG oscillator and the laser diode pumping source.

As in this case, when the sensitivity of the link with one stage of amplification is compared with the two-stage design shown in table 1, the minimum required voltage in node 2 (which is the input to the two-stage amplifier) is about 2 mV. The value measured from figure 27 is about 3.5 mV for the sensitivity of the system with a one-stage amplification. With the proposed noise reduction of the laser source, we expect that the sensitivity of the entire line could be further improved down to 120 μV for the 5-GHz bandwidth, as estimated in table 1.

13. Conclusions

Our experimental results indicate that an externally modulated link with a diode-laser-pumped Nd:YAG laser is capable of achieving broadband performance suitable for measuring wideband signals. As a result of our experiments with the prototype, we determined that the bandwidth could range from 5 to 9 GHz, without the need for additional equalizing circuits. The key component of the system was the New Focus Mach-Zehnder modulator, with a bandwidth of 10.5 GHz, low noise, a large dynamic range, and low insertion loss.

In order to reach the maximum capabilities of the link, we tested two different broadband, high-gain amplifiers. The B&H AC9011H20 amplifier had advantages, such as a gain of 20 dB, a large dynamic range of 96 dB, and a sensitivity of 80 μV at 10 GHz. We measured the 1-dB compression point of the B&H amplifier at 24 dBm, which covers the required dynamic range of the driving stages. This output level enabled the amplifier to drive the modulator hard enough to maximize the modulator's linear dynamic range.

Our second choice for the amplifier stage is the German-made SHF79B amplifier, with a similar bandwidth, a gain of 20 dB, and an output signal of 10 dBm at the 1-dB compression point. This signal-saturation level restricts the dynamic range of the link's second amplification stage that drives the modulator. The primary advantage of the SHF amplifier is its smooth rolloff of the frequency response beyond the –3-dB cutoff point.

There are two issues to be addressed in the Phase II effort of this project in order to improve the performance of the integrated system. First, a large ripple appeared in the frequency response curve at frequencies above 7 GHz. Tests carried out in the Phase I effort indicated that this could be due to optical reflections between the laser and modulator. The use of a fiber-optic isolator at the laser output provides a standard solution that will eliminate or, at the very least, drastically reduce such undesirable feedback signals that perturb the laser oscillator cavity. The second issue is related to the use of a more reliable and accurate polarization-controller unit. The manual polarization controller (MPC1000) used for our work is only adequate for controlled laboratory experiments. Systems based on piezo-electric, servo-controlled, fiber-optic polarizers are more appropriate for field applications. We will incorporate a polarization-maintaining fiber pigtail in the Phase II effort.

The reduction of the noise level and spurious harmonic generation of the cw laser source is also important for the Phase II effort. Several well-proven techniques have been used for reducing spurious signals in commercial laser externally modulated optical links. We will compare and optimize alternative techniques for Army application.

Development of a fiber-optic link with broad bandwidth would significantly enhance the Army's ability to improve the fidelity of transmitted signals. Additionally, such development would greatly benefit the commercial sector, where every 1-GHz bandwidth would accommodate approximately 200 channels of video signals.

References

1. W. K. Burns, T. G. Giallorenzi, R. P. Moeller, and E. J. West, *Interferometric Waveguide Modulator with Polarization-Independent Operation*, Appl. Phys. Lett. **33**, 944 (1978).

2. C. H. Bulmer, W. K. Burns, and R. P. Moeller, *Linear Interferometric Waveguide Modulator for Electro-Magnetic Field Detection*, Appl. Phys. Lett. **53**, 24 (1988).

3. New Focus, Inc., *Integrated Optical Guided Wave Intensity/Phase Modulator* (1993).

4. Hewett Packard, *Fiber-Optic Handbook*.

5. BT&D Technologies, *MPC1000 Manual Polarization Controller*, publication no. 012 (1992).

REPORT DOCUMENTATION PAGE

Form Approved
OMB No. 0704-0188

1. AGENCY USE ONLY *(Leave blank)*	2. REPORT DATE	3. REPORT TYPE AND DATES COVERED
	January 1997	Final, from 1 June 1994–1 June 1996

4. TITLE AND SUBTITLE
High-Sensitivity Wideband Analog Fiber-Optic Link Based on Integrated Optic Modulators

5. FUNDING NUMBERS
PE: 612120

6. AUTHOR(S)
Bruce T. Benwell (ARL), Daniel Edmands and Eduardo Saravia (Interscience, Inc.)

7. PERFORMING ORGANIZATION NAME(S) AND ADDRESS(ES)
U.S. Army Research Laboratory
Attn: AMSRL-WT-NF
2800 Powder Mill Road
Adelphi, MD 20783-1197

8. PERFORMING ORGANIZATION REPORT NUMBER
ARL-TR-1188

9. SPONSORING/MONITORING AGENCY NAME(S) AND ADDRESS(ES)
U.S. Army Research Laboratory
2800 Powder Mill Road
Adelphi, MD 20783-1197

10. SPONSORING/MONITORING AGENCY REPORT NUMBER

11. SUPPLEMENTARY NOTES
AMS code: 612120.1400011
ARL PR: 5FE425

12a. DISTRIBUTION/AVAILABILITY STATEMENT
Approved for public release; distribution unlimited.

12b. DISTRIBUTION CODE

13. ABSTRACT *(Maximum 200 words)*

This report summarizes the design and testing of a 10-GHz analog fiber-optic link. The device is based on a state-of-the-art, commercially available $LiNbO_3$ electro-optic integrated Mach-Zehnder modulator. The performance of the integrated link, as well as each individual component, is characterized and documented.

14. SUBJECT TERMS
Mach-Zehnder modulator, integrated optical modulator

15. NUMBER OF PAGES
34

16. PRICE CODE

17. SECURITY CLASSIFICATION OF REPORT	18. SECURITY CLASSIFICATION OF THIS PAGE	19. SECURITY CLASSIFICATION OF ABSTRACT	20. LIMITATION OF ABSTRACT
Unclassified	Unclassified	Unclassified	UL

NSN 7540-01-280-5500

Standard Form 298 (Rev. 2-89)
Prescribed by ANSI Std. Z39-18
298-102